# Hartree-Fock and lowest-order vertex-correction contribution to the direct gap of the semiconductor silicon

R. Daling and W. van Haeringen
*Eindhoven University of Technology, Department of Physics, P.O. Box 513, 5600 MB, Eindhoven, The Netherlands*
(Received 23 June 1989)

We have calculated the contribution of the second-order vertex-correction diagram to the direct gap of silicon at the Γ point and have compared it with the Hartree-Fock contribution. Both contributions have been calculated by using the Monte Carlo method for the involved three- and six-dimensional integrations. Our results show that the second-order contribution is much smaller than the first-order Hartree-Fock contribution. Although we have calculated the vertex correction diagram using the bare instead of the screened Coulomb interaction, our results give a first indication that vertex corrections can indeed be neglected, an assumption which is inherent in the *GW* approximation to the electron self-energy in a semiconductor.

## I. INTRODUCTION

The problem of dealing with many-particle systems is a longstanding and difficult one. According to quantum mechanics, a many-particle system is described by the many-particle Schrödinger equation. Only in the case of noninteracting particles can this equation be solved because it can trivially be reduced to many identical one-particle equations. When dealing with mutually interacting particles it is impossible to solve the Schrödinger equation, however it is possible to describe the system in terms of quasiparticles whose behavior is governed by a one-(quasi)particle equation. In this equation all many-particle effects are accounted for by an effective one-particle potential function, the so-called self-energy operator ($\hat{M}$), which is both nonlocal and energy dependent. Using this one-(quasi)particle equation, the problem has been shifted from solving the many-particle Schrödinger equation to the determination of the self-energy operator. The determination of the exact $\hat{M}$ is just as impossible as solving the many-particle Schrödinger equation and we have to use some approximation for it. Conceivable approximations for $\hat{M}$ can be obtained by using many-particle perturbation theory which gives a series expansion of $\hat{M}$ in powers of the two-particle interaction. An example of an approximation for $\hat{M}$ which can be obtained in this context is the Hartree-Fock (HF) approximation which corresponds to retaining only the two terms that are of first order in the two-particle interaction.

The approximation for the self-energy operator which one has to use in order to obtain the correct quasiparticle energies will generally depend on the specific many-particle system. The many-particle system we are dealing with in this paper is the semiconductor silicon, the two-particle interaction being the Coulomb interaction between the electrons. As it turns out in band-structure calculations for semiconductors, the HF approximation yields band gaps which are a factor of 2 or more larger than the experimentally observed values,[1,2] whereas recent calculations indicate that for Si use of the so-called *GW* approximation of Hedin[3] for the self-energy operator yields correct band structures.[4–6] This *GW* approximation consists of the first-order term of a perturbation series which has been formulated in powers of a screened interaction *W* rather than in powers of the bare Coulomb interaction (Fig. 1). For an extensive review of many-particle techniques in solid-state physics, see Ref. 7.

Approximating the self-energy operator by *GW* must, of course, be justified. Part of this justification can be based on the successful results of band-structure calculations in which this approximation is used. However, in principle one should show that higher-order contributions in *W* are unimportant with respect to the first-order contribution. It is this latter kind of justification to which we have tried to make a first step by calculating the first-order HF and second-order vertex-correction diagrams and comparing their respective contributions to the direct gap at the Γ point. Because of the complexity

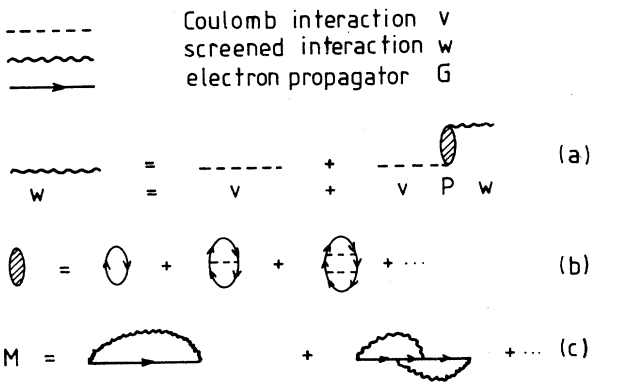


FIG. 1. Summary of the diagrammatic expansion of *M* in powers of the screened interaction *W*. For actual calculations several approximations have to be made; *P* must be approximated giving an approximate *W*. Using this *W*, a choice for *M* has to be made.

 

of the second-order diagrams in $W$, we have used the bare Coulomb interaction instead of the screened interaction. Even then the calculation of especially the second-order contribution appears to be a sizable task. The result clearly indicates that this contribution can safely be disregarded. As the screened interaction $W$ is less effective than the bare interaction $v$, it can be argued that the same result would have been obtained if we had been able to perform the calculations with $W$ instead of $v$. In Ref. 8 a model screened interaction has been used to obtain an estimate for the vertex-correction contribution to the direct gap. The calculation done in Ref. 8 differs from ours in that more approximations have been made, but the conclusion arrived at is basically the same.

## II. BASIC STARTING POINT

In this section we will describe the computational scheme within which it is possible to obtain a reasonable estimate for the importance of the second-order diagram. The determination of the contribution of a certain diagram to the self-energy operator requires in principle a self-consistent calculation. This is so because the self-energy operator, or an approximation for it, is a functional of the one-particle Green's function which in turn depends on the self-energy operator via the one-(quasi)-particle Schrödinger equation. Thus if we want to compare the importance of, e.g., the second-order diagrams with respect to the first-order diagrams, we have to perform two self-consistent calculations, one in which we approximate $\hat{M}$ by the first-order diagrams and one in which we approximate $\hat{M}$ by a sum of the first- and second-order diagrams. Having done these calculations we can decide about the importance of the second-order diagrams by comparing the obtained quasiparticle energies (i.e., band structures). However, performing a completely self-consistent calculation for the electron self-energy is difficult, if not unachievable, certainly if we want to include second-order diagrams. This means that we have to try to circumvent this self-consistency problem. Self-consistency would be no problem if we had disposal of the exact self-consistently determined self-energy operator which could then be used to calculate the exact one-particle Green's function. Using this exact Green's function, we would then be able to calculate any self-energy diagram without having to do a self-consistent calculation. Though in practice the exact self-energy operator is an unknown quantity, we can take the point of view that if we are able to find a Hamiltonian which yields reasonable band structures and electron densities we may use this Hamiltonian as if it contains the exact self-energy operator. Following this line of thought we have used an empirical pseudopotential ($\hat{V}_{\text{emp}}$) and have considered it to be the sum of the crystal potential and the exact self-energy operator. This assumption is expressed in the following equation for the one-(quasi)particle Hamiltonian:

$$\begin{aligned}\hat{H} &= \hat{T} + \hat{V}_{\text{emp}} \\ &= \hat{T} + \hat{U}_{\text{cr}} + (\hat{V}_{\text{emp}} - \hat{U}_{\text{cr}}) \\ &\approx \hat{T} + \hat{U}_{\text{cr}} + \hat{M}_{\text{exact}} \ . \end{aligned} \tag{1}$$

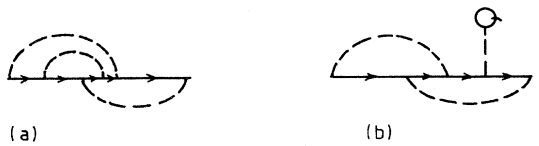


FIG. 2. Example of a skeleton (a) and a nonskeleton (b) diagram.

In this equation $\hat{T}$ is the kinetic energy operator and $\hat{U}_{\text{cr}}$ is the crystal potential. Using the one-particle Green's function corresponding to this Hamiltonian, we have calculated the relevant first- and second-order diagrams. Which diagrams we have to calculate in order to be consistent with the assumption that the Hamiltonian of Eq. (1) yields the exact Green's function will be discussed in the next section.

## III. DIAGRAMS TO BE CALCULATED

If the diagrammatic expansion of the self-energy operator is written down using the *exact* one-(quasi)particle Green's function, only the so-called skeleton diagrams must be included. A skeleton diagram is defined as a diagram without a self-energy correction to any of its internal propagators. For example, the diagram of Fig. 2(a) is a skeleton diagram whereas the diagram of Fig. 2(b) is not because it contains a Hartree self-energy correction to one of its internal propagators. In accordance with this and the assumption concerning our use of the empirical pseudopotential, we have to consider only skeleton diagrams if we want to compare the importance of first- and second-order diagrams. It is to be noted in this connection that a subset of the class of skeleton diagrams consists of diagrams that contain polarization parts in their interaction lines (Fig. 3). The only second-order diagram of this kind is depicted in Fig. 3(a). If the perturbation expansion for $\hat{M}$ is formulated in powers of $W$, diagrams with the topology as in Fig. 3 will not be encountered. Henceforth, we will simply discard the diagram of Fig. 3(a) and consider only the second-order diagrams that appear if $\hat{M}$ is expanded in powers of $W$, however with $W$ replaced by the bare Coulomb interaction.

The first- and second-order skeleton diagrams which

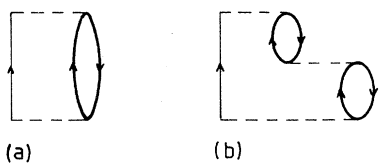


FIG. 3. Examples of skeleton diagrams which contain polarization parts in their interaction lines.

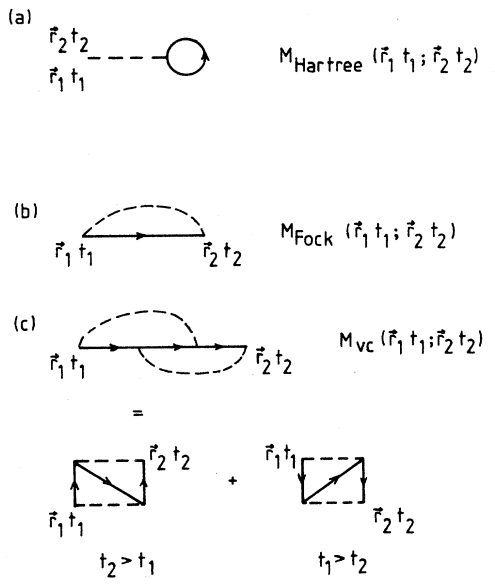


FIG. 4. The first- and second-order contributions to the self-energy operator which we have calculated.

we have to calculate are shown in Fig. 4. The second-order diagram has been split into two contributions according to the two possible time orderings of its arguments. When written down in the Fourier domain, the second-order diagram will be frequency (energy) dependent whereas the HF diagrams will be energy indepenent.

## IV. NUMERICAL EVALUATION

As discussed in Sec. II, we use an empirical pseudopotential to calculate the Green's function which is needed to calculate the diagrams. The parameters that we have used in this pseudopotential are given in Table I and have been taken from Ref. 9.

We have determined the matrix elements of the self-energy operator in a plane-wave representation:

$$M(\mathbf{k}+\mathbf{K}_1,\mathbf{k}+\mathbf{K}_2,\omega)=\langle \mathbf{k}+\mathbf{K}_1|\hat{M}(\omega)|\mathbf{k}+\mathbf{K}_2\rangle \ , \quad (2)$$

in which $\mathbf{k}$ lies in the first Brillouin zone (1BZ), $\mathbf{K}_1$ and $\mathbf{K}_2$ are reciprocal-lattice vectors, and $\omega$ is the energy parameter. In Appendix A we display again the three relevant diagrams of Fig. 4 and give the corresponding expressions. The Hartree contribution depends neither on $\mathbf{k}$ nor on $\omega$, while the Fock contribution depends on $\mathbf{k}$ but not on $\omega$.

The evaluation of Feynman diagrams involves the summation over intermediate states or, when we are dealing with an infinite system, an integration over intermediate states. For the two first-order diagrams of Fig. 4 this implies that we have to perform one band summation and one (crystal) momentum integration over 1BZ. The second-order diagram of Fig. 4 contains two-particle–one-hole or one-particle–two-hole intermediate states implying three band summations and three momentum integrations. One of the three momentum integrations can be performed analytically using the $\delta$ functions which express momentum conservation at the interaction vertices. This leaves us with three band summations and a six-dimensional integral over the direct product of two 1BZ's. The momentum integrations have been performed using a Monte Carlo integration procedure. The random points which are needed for this integration procedure have been generated by using the Halton sequence as described in Ref. 10.

From the expressions in (A4) and (A7) in Appendix A, we see that both the Fock and the vertex-correction diagram have integrands containing singularities arising from the Coulomb potential. In the case of the Fock diagram we have one singularity at $\mathbf{q}=\mathbf{0}$ [see (A4) and consider the $\mathbf{Q}=\mathbf{0}$ term]. To make numerical integration possible we subtract from the integrand a singular function such that the difference is a regular function which can easily be integrated numerically. The subtracted function is chosen in such a way that it can be integrated analytically over 1BZ (see Appendix B). The terms in the integrand of the vertex-correction diagram with $\mathbf{Q}_1=\mathbf{K}_2$ or $\mathbf{Q}_3=\mathbf{K}_1$ are singular whenever $\mathbf{q}_1=\mathbf{k}$ or $\mathbf{q}_2=\mathbf{k}$. These singularities are less severe than the singularity in the Fock diagram due to the fact that if we take $\mathbf{q}_1=\mathbf{k}$ the numerator in the singular term in Eq. (A7) also vanishes because in that case it is proportional to the inner product between a valence-band state and a conduction-band state at the same point in the 1BZ. A similar observation holds for the case $\mathbf{q}_2=\mathbf{k}$. We have treated these singularities by performing a Monte Carlo sampling using points $(\mathbf{q}_1,\mathbf{q}_2)$ which are uniformly distributed in polar coordinates $(r_1,\theta_1,\phi_1,r_2,\theta_2,\phi_2)$; this implies that we have to multiply the integrand by a Jacobian containing factors which cancel the Coulomb singularities. In this way there are effectively no singularities in the integrand. This method has one drawback caused by the fact that it is cumbersome to give 1BZ in terms of polar coordinates. A solution to this problem is to enclose 1BZ×1BZ by the direct product of two spheres and to define a new function which is equal to the original integrand in the intersection of the spheres and 1BZ×1BZ and zero otherwise. The integral of this new function over the direct product of the two spheres is by definition the same as the integral we want to calculate. However, our new function has a discontinuity on the boundary of 1BZ×1BZ. In principle discontinuities do not present problems for a Monte Carlo integration, but if we use the variance of the sampled function values to estimate the error in our final results part of this error will be due to this discontinuity. We have estimated the absolute error in our Monte Carlo integration results by the square root of the sample variance divided by the square root of the number of integration points.

TABLE I. Empirical pseudopotential parameters in Ry. $V_{emp}(\mathbf{K})=\cos(\mathbf{K}\cdot\mathbf{t})\phi(|\mathbf{K}|)$ and $\mathbf{t}=(a/8)(\mathbf{x}+\mathbf{y}+\mathbf{z})$.

| $\phi(\sqrt{3})$ | $\phi(\sqrt{8})$ | $\phi(\sqrt{11})$ |
|---|---|---|
| −0.224 | 0.055 | 0.072 |

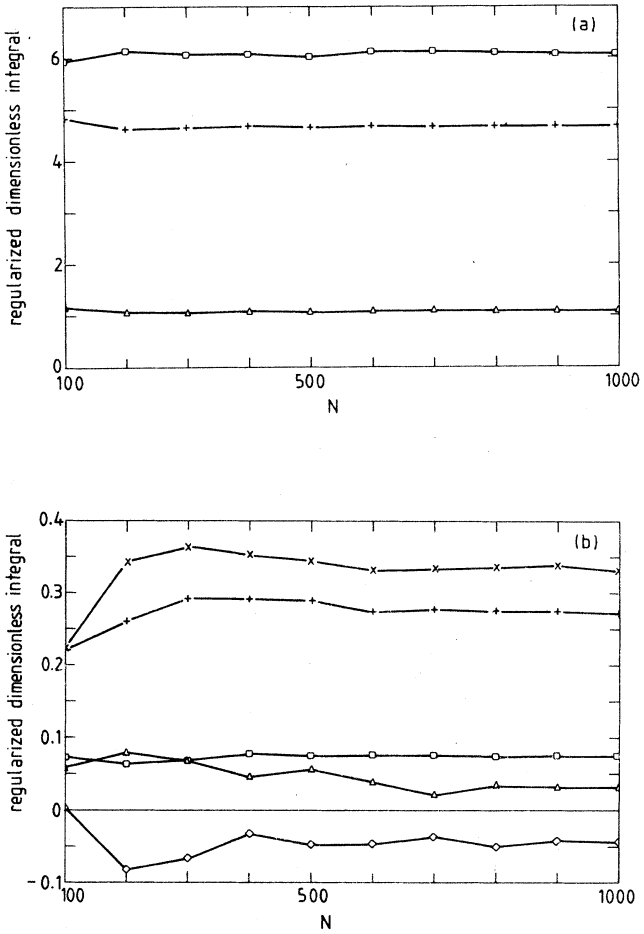


FIG. 5. Monte Carlo estimate for the regularized integral of the Fock diagram (see Appendix B) as function of the number of random points. The curves correspond to the eight independent matrix elements which contribute to the direct gap (see text). In (a): □=(111),(111); +=(011),(011); △=(111),(011). In (b): ×=(−1−1−1),(100); +=(−1−1−1),(101); □=(101),(−10−1); △=(−1−1−1),(00−1); ◇=(−1−1−1),(111).

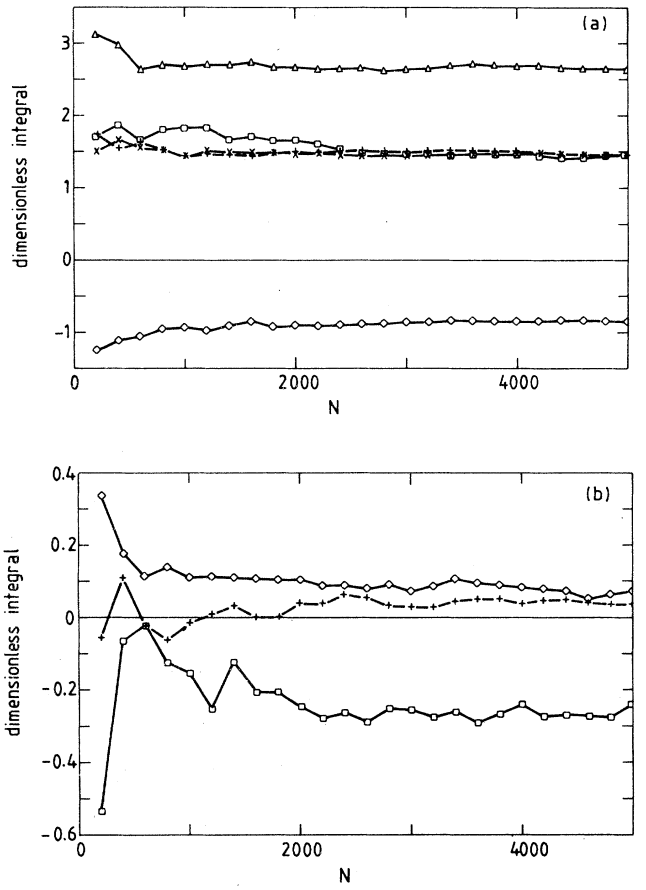


FIG. 6. Monte Carlo estimate for the integral appearing in the expression for the vertex correction diagram [Eqs. (A6) and (A7)] as a function of the number of random points. The energy parameter corresponds to the energy of the highest valence-band state $\Gamma'_{25}$. The curves correspond to the eight independent matrix elements which contribute to the direct gap (see text). In (a): △=(011),(011); □=(111)(111); ×=(101),(−10−1); +=(−1−1−1),(111); ◇=(111),(011). In (b): ◇=(−1−1−1),(101); +=(−1−1−1),(00−1); □=(−1−1−1),(100).

Because of the large number of summations that has to be performed to calculate the integrand of Eq. (A7) we have to restrict ourselves to a small number of bands. We have done our calculations using a 15-band model so that the matrix $M$ consists of 225 elements for each $\mathbf{k}$ and $\omega$ value. Using the symmetry group at the $\Gamma$ point it can be shown that the number of independent elements is only 16. The symmetry property of $M$ under interchange of $\mathbf{K}_1$ and $\mathbf{K}_2$ reduces this to 12 elements, one of which can be shown to be exactly zero. Of the remaining 11 elements only eight contribute to the direct gap at $\mathbf{k}=0$.

In Figs. 5–7 we present some results concerning the Monte Carlo integration procedure. In Fig. 5 the Monte Carlo estimate for the regularized integral, i.e., the integral of (A4) with (B1) subtracted from its integrand, appearing in the expression for the Fock diagram has been plotted as a function of the number of integration points. The curves correspond to those eight matrix elements which contribute to the direct gap at $\mathbf{k}=0$. We see that the convergence of the estimate is good especially for the large diagonal elements. The estimated errors on the results which we have obtained using 1000 integration points vary between 2% and 7%. In Figs. 6 and 7 the results for the vertex-correction diagram are shown. To estimate the integrals we have used 5000 random points which have been sampled uniformly in polar coordinates. This yielded results which are accurate enough for our purpose, which is to give a rough estimate for the ratio of second-order to first-order expectation values. Figure 7 demonstrates the correctness of our integration procedure by showing that different sets of random points converge to the same estimate for the integral. Note that 6000 integration points for a six-dimensional integral is a rather modest value corresponding to about 4.25 points per dimension. The evaluation of the necessary matrix elements of the second-order diagram using 5000 integration points required 104 h of computation time on an IBM-RT system.

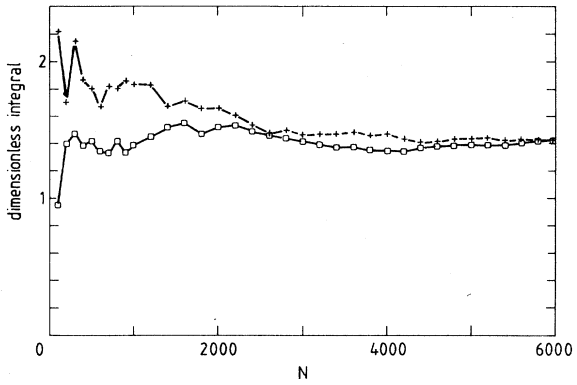


FIG. 7. Estimate for the second-order matrix element (111),(111) as a function of the number of random points for two different sets of random points. The energy parameter corresponds to the energy of the highest valence-band state $\Gamma'_{25}$.

## V. RESULTS

In order to have some kind of a check on the credibility of our results, we compare in Table II our HF results with results obtained by other authors. In order to be consistent with our assumptions concerning the empirical pseudopotential,

$$\hat{V}_{\text{emp}} = \hat{U}_{\text{cr}} + \hat{M}_{\text{exact}} = \hat{U}_{\text{cr}} + \hat{M}_{\text{HF}} + \hat{M}_{\text{rest}} \ , \tag{3}$$

we have to calculate our HF energies by taking the expectation values of $\hat{T}+\hat{U}_{\text{cr}}+\hat{M}_{\text{HF}}$ in the eigenstates of $\hat{T}+\hat{V}_{\text{emp}}$. For $\hat{U}_{\text{cr}}$ we have used the *ab initio* ion potential of Ref. 11. Note that our HF energies have not been obtained by a fully self-consistent "HF only" calculation, but have in our scheme to be interpreted as the HF contribution to the band structure as obtained with the exact $\hat{M}$ of which HF is only a part. From Table II we see that our results are in reasonable agreement with the results of other calculations and we conclude that our way of working yields reasonable estimates for at least the first-order diagrams. Comparing the first and second columns in Table II we see that $(\hat{V}_{\text{emp}}-\hat{U}_{\text{cr}})$ must contain more than $\hat{M}_{\text{HF}}$, i.e., the higher-order diagrams contributing to $\hat{M}_{\text{exact}}$ which are denoted as $\hat{M}_{\text{rest}}$ in Eq. (3) cannot all be small with respect to the first-order HF contribution.

In Table III the expectation values of the vertex-correction diagram in the lowest conduction-band state in $\Gamma$ ($\Gamma_{15}$) and in the highest valence-band state ($\Gamma'_{25}$) are compared with those of the HF diagrams in the same states. We see that the second-order expectation values are, respectively, factors of 18 and 37 smaller than the first-order expectation values in the $\Gamma_{15}$ and the $\Gamma'_{25}$ states. Although the second-order contribution to the direct gap at the $\Gamma$ point is in fact undetermined due to the large cancellation that occurs when we calculate the difference of the expectation values in the $\Gamma_{15}$ and in the $\Gamma'_{25}$ states, we conclude that the HF contribution to the direct gap at the $\Gamma$ point is at least a factor of 36 larger than the contribution of the vertex-correction diagram. From Table II and use of (3) we learn that the contribution of $\hat{M}_{\text{rest}}$ to the direct gap is $-5.71$ eV $[\hat{M}_{\text{rest}}=(\hat{T}+\hat{V}_{\text{emp}})-(\hat{T}+\hat{M}_{\text{HF}}+\hat{U}_{\text{cr}})]$. As we have shown in Table III the second-order vertex correction does not yield this large contribution and therefore other higher-order diagrams in $\hat{M}_{\text{rest}}$ must give this contribution to the direct gap and these must be the diagrams which are taken into account in the *GW* approximation. Because of the fact that in the *GW* approximation the Hartree term is not modified and the fact that this approximation gives correct band structures, we conclude that the *GW* diagram of Fig. 1(c) contributes about $\hat{M}_{\text{rest}}+\hat{M}_{\text{Fock}}=0.54$ eV to the direct gap which is a factor of 11 smaller than the *Gv* (Fock) contribution. This factor of 11 should be compared with the dielectric constant $\epsilon_0$ of Si which is 12.

TABLE II. Hartree-Fock energies (eV) compared with values obtained by other authors.

| | $T+V_{\text{emp}}$ | $T+U_{\text{cr}}+M_{\text{HF}}$ | (a) | (b) |
|---|---|---|---|---|
| $\Gamma_{15}-\Gamma'_{25}$ | 3.47 | 9.18 | 8.0 | 9.4 |
| $\Gamma'_{25}-\Gamma_1$ | 12.97 | 17.3 | 18.3 | 19.8 |

[a]Reference 1.
[b]R. Dovesi, M. Causa, and G. Angonoa, Phys. Rev. B **24**, 4177 (1981).

TABLE III. Expectation values of the first- and second-order diagrams and contributions to the direct gap at $\Gamma$. Energies are in eV and numbers in parentheses are estimated relative errors.

| | $M_{\text{Hartree}}$ | $M_{\text{Fock}}$ | $M_{\text{HF}}$ | $M_{\text{VC}}$ |
|---|---|---|---|---|
| $\Gamma_{15}$ | 0.041(14) | −5.35(2.7) | −5.31(2.8) | 0.284(10) |
| $\Gamma'_{25}$ | 2.67(1.1) | −11.6(1.2) | −8.93(1.7) | 0.237(10) |
| $\Gamma_{15}-\Gamma'_{25}$ | −2.63(1.3) | 6.25(4.6) | 3.62(8.3) | 0.047(100) |

## VI. CONCLUSIONS

As mentioned in the Introduction a large step towards the justification of the *GW* approximation would be an explicit demonstration of the smallness of the vertex-correction diagram of Fig. 1(c) with respect to the *GW* diagram of Fig. 1(c). We have argued in the Introduction that if this can be shown for diagrams with the bare Coulomb interaction $v$ this will very likely be true for diagrams containing screened interactions $W$ as well.

Our calculations show that contribution to the direct gap of the second-order self-energy diagram of Fig. 4(c) is indeed much smaller than the first-order HF contribution. Furthermore, if we assume that the correct energy gap is indeed produced with the *GW* approximation, we conclude that the ratio of the *Gv* (Fock) to the *GW* contribution to the energy gap is about 11, which is fully in accordance with the idea of a sizable effective screening contained in the function $W$.

Strictly speaking, the relative smallness of the screened vertex-correction diagram has still to be demonstrated, though the relative "weakness' of $W$ with respect to $v$ strongly suggests this to be the case. Unfortunately, one


FIG. 8. Symbols used in Feynman diagrams of Appendix A.

of the consequences of the dynamic character of $W$ is that the vertex-correction diagram of Fig. 1(c) gives rise to 24 different diagrams corresponding to the 4! different time orderings in which the vertices of the screened interaction can be arranged. Each of these diagrams will be much more difficult to evaluate than the diagrams that we have calculated thus far, even if we use a simple plasmon pole approximation for the screened interaction.[12] In conclusion, we believe that the accurate evaluation of the ratio of the unscreened Fock and vertex-correction diagrams makes it very likely that higher-order vertex-correction diagrams in the screened interaction can indeed be neglected in the evaluation of an energy gap in semiconductors such as Si.

## APPENDIX A

In this Appendix we give the expressions corresponding to the three self-energy diagrams which we have calculated. We use the following conventions.

(i) Momenta are measured in units of $2\pi/a$ in which $a$ is the silicon lattice constant, $a=5.43$ Å.

(ii) Energies are measured in units of $E_v=2\pi^2\hbar^2/ma^2$, $E_v=0.375$ Ry.

(iii) In Feynman diagrams the following symbols are used: in Fig. 8(a), the Coulomb interaction $e^2/\epsilon_0|\mathbf{q}|^2$; in Fig. 8(b), the one electron propagator in which the change of the electron momentum by a reciprocal-lattice vector $\mathbf{K}$ is explicitly depicted.

(iv) $d_{1\mathbf{k}}(\mathbf{K})$ is a plane-wave coefficient; because we have chosen the origin in a bond center these coefficients are real.

(v) VB is for valence bands and CB is for conduction bands.

The Hartree diagram in Fig. 9(a) is

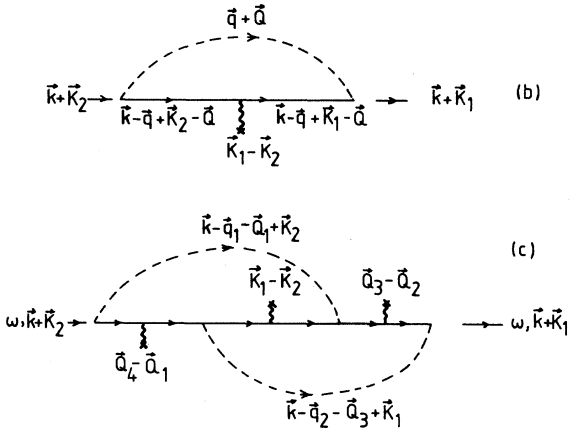


FIG. 9. The diagrams which we have calculated in momentum representation. The corresponding expressions are given in Sec. (A1)–(A7).

$$M_{\text{Hartree}}(\mathbf{K}_1,\mathbf{K}_2)=\frac{E_v}{\hbar}\left[\frac{e^2}{4\pi^2\epsilon_0 aE_v}\right]I_{\text{Hartree}}(\mathbf{K}_1,\mathbf{K}_2)\ . \tag{A1}$$

$I_{\text{Hartree}}(\mathbf{K}_1,\mathbf{K}_2)$ is a dimensionless integral given by

$$I_{\text{Hartree}}(\mathbf{K}_1,\mathbf{K}_2)=\int_{1\text{BZ}}d^3q\sum_{l\in\text{VB}}\sum_{\mathbf{Q}}\frac{d_{l\mathbf{q}}(\mathbf{Q}+\mathbf{K}_1)d_{l\mathbf{q}}(\mathbf{Q}+\mathbf{K}_2)}{|\mathbf{K}_1-\mathbf{K}_2|^2} \tag{A2}$$

and $e^2/4\pi^2\epsilon_0 aE_v=0.1653$ is a dimensionless constant.

The Fock diagram in Fig. 9(b) is

$$M_{\text{Fock}}(\mathbf{k}+\mathbf{K}_1,\mathbf{k}+\mathbf{K}_2)=-\frac{E_v}{\hbar}\left[\frac{e^2}{4\pi^2\epsilon_0 aE_v}\right]I_{\text{Fock}}(\mathbf{k}+\mathbf{K}_1,\mathbf{k}+\mathbf{K}_2)\ , \tag{A3}$$

$$I_{\text{Fock}}(\mathbf{k}+\mathbf{K}_1,\mathbf{k}+\mathbf{K}_2)=\int_{1\text{BZ}}d^3q\sum_{l\in\text{VB}}\sum_{\mathbf{Q}}\frac{d_{l\mathbf{k}-\mathbf{q}-\mathbf{R}}(\mathbf{K}_1-\mathbf{Q}+\mathbf{R})d_{l\mathbf{k}-\mathbf{q}-\mathbf{R}}(\mathbf{K}_2-\mathbf{Q}+\mathbf{R})}{|\mathbf{q}+\mathbf{Q}|^2}\ . \tag{A4}$$

$\mathbf{R}$ is a reciprocal-lattice vector such that $\mathbf{k}-\mathbf{q}-\mathbf{R}\in 1\text{BZ}$.

The vertex-correction diagram in Fig. 9(c) is

$$M_{\text{VC}}(\mathbf{k}+\mathbf{K}_1,\mathbf{k}+\mathbf{K}_2,w)=-\frac{E_v}{\hbar}\left[\frac{e^2}{4\pi^2\epsilon_0 aE_v}\right]^2 I_{\text{VC}}(\mathbf{k}+\mathbf{K}_1,\mathbf{k}+\mathbf{K}_2,w)\ , \tag{A5}$$

$$I_{\text{VC}}(\mathbf{k}+\mathbf{K}_1,\mathbf{k}+\mathbf{K}_2,\omega)=I^1_{\text{VC}}(\mathbf{k}+\mathbf{K}_1,\mathbf{k}+\mathbf{K}_2,\omega)+I^2_{\text{VC}}(\mathbf{k}+\mathbf{K}_1,\mathbf{k}+\mathbf{K}_2,\omega)\ , \tag{A6}$$

$$I^1_{\mathrm{VC}}(\mathbf{k}+\mathbf{K}_1,\mathbf{k}+\mathbf{K}_2,\omega)=\int_{1\mathrm{BZ}} d^3q_1 \int_{1\mathrm{BZ}} d^3q_2 \sum_{l_1\in\mathrm{CB}} \sum_{l_2\in\mathrm{VB}} \sum_{l_3\in\mathrm{CB}} \frac{1}{\omega-\epsilon_{l_1}(\mathbf{q}_1)+\epsilon_{l_2}(\mathbf{q}_1+\mathbf{q}_2-\mathbf{k}-\mathbf{R})-\epsilon_{l_3}(\mathbf{q}_2)+i\eta}$$
$$\times\sum_{\mathbf{Q}_1}\frac{d_{l_1\mathbf{q}_1}(\mathbf{Q}_1)}{|\mathbf{k}-\mathbf{q}_1-\mathbf{Q}_1+\mathbf{K}_2|^2}\sum_{\mathbf{Q}_2} d_{l_3\mathbf{q}_2}(\mathbf{Q}_2)d_{l_2\mathbf{q}_1+\mathbf{q}_2-\mathbf{k}-\mathbf{R}}(\mathbf{Q}_1+\mathbf{Q}_2-\mathbf{K}_2+\mathbf{R})$$
$$\times\sum_{\mathbf{Q}_3}\frac{d_{l_3\mathbf{q}_2}(\mathbf{Q}_3)}{|\mathbf{k}-\mathbf{q}_2-\mathbf{Q}_2+\mathbf{K}_1|^2}\sum_{\mathbf{Q}_4} d_{l_1\mathbf{q}_1}(\mathbf{Q}_4)d_{l_2\mathbf{q}_1+\mathbf{q}_2-\mathbf{k}-\mathbf{R}}(\mathbf{Q}_4+\mathbf{Q}_3-\mathbf{K}_1+\mathbf{R})\ . \quad \text{(A7)}$$

The expression for $I^2_{\mathrm{VC}}$ is the same as for $I^1_{\mathrm{VC}}$, however, with the summation over the valence bands replaced by a summation over the conduction bands and vice versa. Besides, $i\eta$ has to be replaced by $-i\eta$.

## APPENDIX B

The singularity in the integrand of the Fock diagram can be handled by subtracting the following function from the integrand in Eq. (A4):

$$S(\mathbf{K}_1,\mathbf{K}_2,\mathbf{k};\mathbf{q})=\sum_{l\in\mathrm{VB}}\frac{d_{l\mathbf{k}}(\mathbf{K}_1)d_{1\mathbf{k}}(\mathbf{K}_2)}{|\mathbf{q}|^2}\frac{1}{2}\left[1+\cos\left[\frac{\pi|\mathbf{q}|}{b}\right]\right]\Theta(b-|\mathbf{q}|)\ . \quad \text{(B1)}$$

The parameter $b$ should be chosen such that the whole sphere with radius $b$ is contained within the 1BZ.

The difference of the integrand in Eq. (A4) and $S(\mathbf{K}_1,\mathbf{K}_2,\mathbf{k};\mathbf{q})$ is a continuous function without singularities and can easily be integrated numerically. Because of the $\Theta$ function the integral of the singular function $S$ over the 1BZ can easily be determined analytically and is given by

$$\int_{1\mathrm{BZ}} d^3q\, S(\mathbf{K}_1,\mathbf{K}_2,\mathbf{k};\mathbf{q})=2\pi b\sum_{l\in\mathrm{VB}} d_{l\mathbf{k}}(\mathbf{K}_1)d_{l\mathbf{k}}(\mathbf{K}_2)\ . \quad \text{(B2)}$$


[1] W. v. d. Linden, P. Fulde, and K. P. Bohnen Phys. Rev. B **34**, 1063 (1986).
[2] F. Gygi and A. Baldereschi, Phys. Rev. B **34**, 4405 (1986).
[3] L. Hedin, Phys. Rev. **139**, A796 (1965).
[4] M. S. Hybertson and S. G. Louie, Phys. Rev. B **34**, 5390 (1986).
[5] R. W. Godby, M. Schlüter, and L. J. Sham, Phys. Rev. B **37**, 101 59 (1988).
[6] W. v. d. Linden and P. Horsch, Phys. Rev. B **37**, 8351 (1988).
[7] J. C. Inkson, *Many-Body Theory of Solids* (Plenum, New York, 1984).
[8] M. Bennett, J. Phys. C **11**, L515 (1978).
[9] J. R. Chelikowsky and M. L. Cohen, Phys. Rev. B **14**, 556 (1976).
[10] J. Halton, Numer. Math **2**, 84 (1960).
[11] G. B. Bachelet, H. S. Greenside, G. A. Baraff, and M. Schlüter, Phys. Rev. B **24**, 4745 (1981).
[12] We have made an estimate which indicates that the evaluation of the second-order $W$ diagram requires at least 133 d on an IBM-RT system.